ISSN 2616-5767 Vol.4, Issue 3: 33-51, DOI: 10.25236/AJETS.2021.040305

Study of the Difference between Single and Multi-component Calibration Results of Tire Six-component Force Sensor

Yong Wei*, Yonghui Jia, Baolv Wei

SAIC GM Wuling Automobile Co., Ltd., No.18 Hexi Road, Liunan District, Liuzhou, Guangxi Zhuang Autonomous Region, 545007, PR China
**Corresponding author: yong.wei@sgmw.com.cn*

Abstract: *The paper studies the difference between single and multi-component calibration results of tire six-component force sensor. In accordance with the measuring principle of strain gauge, the different formulas of single calibration and multi-component calibration for one strain gauge are deduced. Taking the resistance strain tire six-component force sensor with four column structure as an example, some certain channel output shows a larger error between single and multi-component calibration results, which is the integrated result of structure and measuring bridge. Because of the difference between the two results, single calibration is not better than multi-component calibration when calibrating a sensor working under multi-component force conditions. The simulation experiments of virtual single and multi-component calibrations are conducted based on Hypermesh and Abaqus. Thus, the above conclusions are confirmed by simulation results. In accordance with the verification above, a more reasonable method for tire six-component force sensor calibration is proposed in this paper.*

Keywords: *tire six-component force sensor, single and multi-component calibration, measuring principle, simulation*

1. Introduction

Tire mechanical properties are closely related to the vehicle performance. Thus, high-precision tire model is indispensable in automobile development. [1] The establishment of current popular tire models, such as Magic Formula and FTire, requires a high-precision six-component force sensor to measure tire six-component force characteristics at the contact patch center or the wheel center under complex motion conditions. [2] [3]

In the manufacturing process of the six-component force sensor, there are many factors that can influence the precision, such as structure design, material heat treatment, machining accuracy, the quality of pasting strain gauges, signal acquisition and processing, etc. They make the mutual coupling between each channel output signal of sensor. The coupling relationship is complicated, so it is difficult to precisely described theoretically. To get the real properties, the actual sensor calibration method is usually adopted, and the calibration precision directly affects the precision of sensor. [4-6] Currently, there are two common calibration methods, single-component calibration method and multi-component calibration method. [7-16] There have been many researches and productions which were calibrated in these two methods by using single or multi-components calibration equipment.

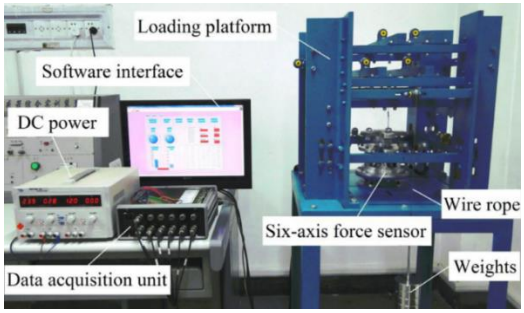

Figure 1. The loading device for calibration experiment in Parallel Robot and Mechatronic System Laboratory of Hebei Province, Yanshan University

ISSN 2616-5767 Vol.4, Issue 3: 33-51, DOI: 10.25236/AJETS.2021.040305

Jiantao Yao and Dajun Cai, et al. [11] from Parallel Robot and Mechatronic System Laboratory of Hebei Province used a weights-loaded device to calibrate a six-axis wrist force sensor. The device is as shown in Figure 1.

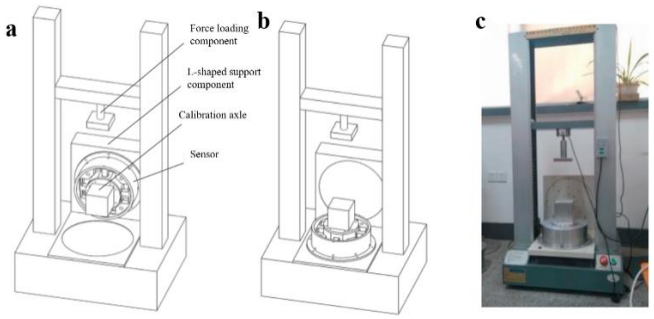

Figure 2. Force calibration system based on material testing machine in School of Instrument Science and Engineering Southeast University. (a) calibration of F_x/F_y; (b) calibration of F_z; (c) photo of the system

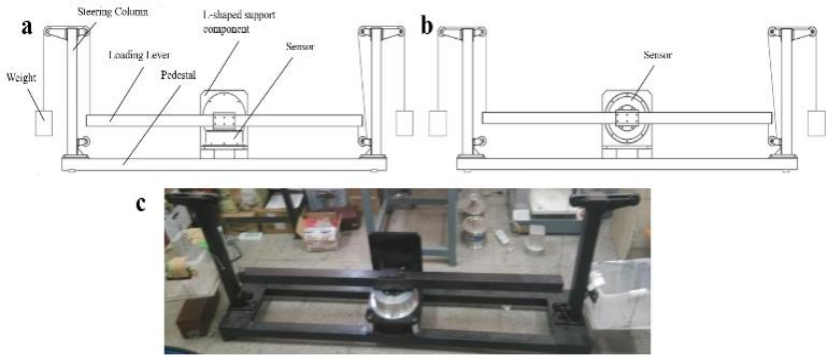

Figure 3. Moment calibration system based on calibration experiment setup in School of Instrument Science and Engineering Southeast University. (a) calibration of M_x/M_y; (b) calibration of M_z; (c) photo of the system

Danfeng Chen and Aiguo Song, et al. [11] from school of instrument science and engineering, Southeast University used two setups to calibrate the six-axis force/moment sensor. As is shown in Figure 2, the forces calibration equipment was based on material testing machine, which can add load continuously. As is shown in Figure 3, the moments were calibrated in a weights-loaded way.

Figure 4. Hexapod calibration device in TU Braunschweig, Institut für Produktionsmesstechnik, Braunschweig, Germany

ISSN 2616-5767 Vol.4, Issue 3: 33-51, DOI: 10.25236/AJETS.2021.040305

Compared with single-component calibration equipment, there are less multi-component calibration equipment. Hexapod-structured is often used because it can realize the loading and motion in six degrees at the same time. [14] J Nitsche and S Baumgarten, et al. [15] designed a hexapod-structured calibration device for multi-component force and moment sensors, just as shown in Figure 4. The machine can generate and measure forces of up to $10kN$ and moments of up to $1kN\ m$.

Figure 5. Kistler's hexapod calibration system in Production Centers

As shown in Figure 5, Kistler has a hexapod calibration system.[16] This system locates in Germany. Its force calibrating range is $\pm 50kN$ and moment calibration range is $\pm 10kN\ m$. It is used to calibrate their production and provide calibration service for customers.

Calibration matrixes obtained by the two calibration methods are not the same. [17] Most six-component force sensor productions are calibrated by the single-component calibration method, for it's low-budget and easy to operate. But in fact, the six-component force sensor productions always work under the multi-component action conditions. [18] In this paper, the difference between single and multi-component calibration is analyzed by taking a resistance strain tire six-component force sensor with four column structure as an example.

The remainder of this paper is organized as follows. Firstly, the measuring principle of resistance strain six-component force sensor is introduced, including the measuring principle of strain gauge, the measuring bridge and the calibration matrix. Secondly, a preliminary conclusion that the result between single and multi-component calibration is different is drew by theoretical analysis. Thirdly, virtual calibrations of single and multi-component methods are carried out by means of finite element analysis. Finally, a more reasonable method for tire six-component force sensor calibration is proposed.

2. Measuring Principle of Resistance Strain Six-component Force Sensor

Resistance strain six-component force sensor is a broad-spectrum force sensor with simple structure. It is composed of elastic component, resistance strain gauges and other accessories. When the elastic component undergoes deformation under load, strain gauges pasting on it have deformation concomitantly. Thus, the resistance of strain gauges changes. [19] As strain gauges are inserted in the circuit, the output voltage of whole circuit changes too. The variation of output voltage respects the magnitude of load.

2.1 Measuring Principle of Resistance Strain Gauge

Resistance strain gauge is the sensing element of force sensor, which is pasted on the elastic component. It is composed of basement, sensitive grid, adhesive, lead and covering layer. [20] [21] Liner strain gauge and torsion/shear strain gauge [22] are widely used in six-component force sensor. Their diagrams are shown in Figure 6.

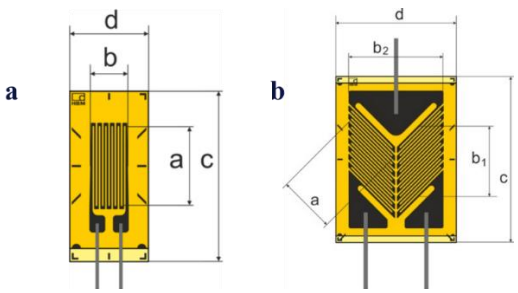

Figure 6. Liner strain gauge and torsion/shear strain gauge. (a) Liner strain gauge (b) Torsion/shear strain gauge

ISSN 2616-5767 Vol.4, Issue 3: 33-51, DOI: 10.25236/AJETS.2021.040305

The relationship between deformation and resistance variation of resistance strain gauge is as follows. [19]

$$\frac{\Delta R}{R} = K\frac{\Delta L}{L} \tag{1}$$

Where R is the resistance of strain gauge with no deformation. ΔR is the variation of resistance.K is the sensitivity coefficient of strain gauge, which can be treated as a constant. L is the length of sensitive grid with no deformation. ΔL is the variation of sensitive grid length.

2.2 Measuring Principle of Bridge

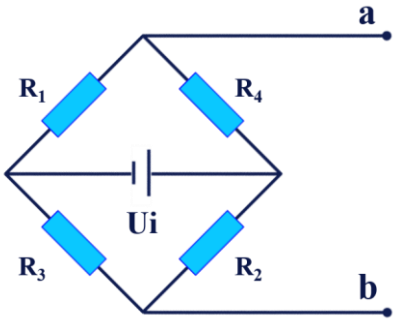

Figure 7. Wheatstone bridge

Wheatstone bridge is a circuit which has four "beams". Each beam has one or more resistances (here we use strain gauges). The relationship between its input voltage and output voltage is as follows. [23-24]

$$U_o = \frac{U_i}{4}\left(\frac{\Delta R_1}{R_1} + \frac{\Delta R_2}{R_2} - \frac{\Delta R_3}{R_3} - \frac{\Delta R_4}{R_4}\right) \tag{2}$$

Where U_o is the output voltage (voltage between node a and node b). U_i is the input voltage.R_1 to R_4 are resistances of strain gauges. ΔR_1 to ΔR_4 are their variation of resistance.

2.3 Calibration Matrix

Calibration matrix is the relationship between load and six-component force sensor output voltage, which is shown in equation 3 and 4 [25-26].

$$\begin{bmatrix} U_1 \\ U_2 \\ U_3 \\ U_4 \\ U_5 \\ U_6 \end{bmatrix} = \begin{bmatrix} C_{11} & C_{21} & C_{31} & C_{41} & C_{51} & C_{61} \\ C_{12} & C_{22} & C_{32} & C_{42} & C_{52} & C_{62} \\ C_{13} & C_{23} & C_{33} & C_{43} & C_{53} & C_{63} \\ C_{14} & C_{24} & C_{34} & C_{44} & C_{54} & C_{64} \\ C_{15} & C_{25} & C_{35} & C_{45} & C_{55} & C_{65} \\ C_{16} & C_{26} & C_{36} & C_{46} & C_{56} & C_{66} \end{bmatrix} \begin{bmatrix} F_x \\ F_y \\ F_z \\ M_x \\ M_y \\ M_z \end{bmatrix} \tag{3}$$

For the sake of writing convenience, equation 3 can also be written as follows:

$$U = CF. \tag{4}$$

Where $F_x, F_y, F_z, M_x, M_y, M_z$are the three forces and three moments loaded on six-component force sensor. U_1 to U_6 are the output voltage of each measuring bridge corresponding with$F_x, F_y, F_z, M_x, M_y, M_z$ one by one.$C_{ij}(i = 1,2 \cdots 6, j = 1,2 \cdots 6)$ is the coefficient of forces and moments worked on output voltage.i refers to the input load and j refers to the output voltage. For example,$C_{23}$is the coefficient that F_y works on U_3. During the calibration process, matrix C can be solved. During the usage of six-component force sensor, the values of U and C are known primarily. Afterwards, F will be calculated.

$$F = C^{-1}U \tag{5}$$

Where C^{-1} is just the calibration matrix. Single and multi-component calibration method can both get C^{-1} by getting C at first.

1) Single-component Calibration Method

ISSN 2616-5767 Vol.4, Issue 3: 33-51, DOI: 10.25236/AJETS.2021.040305

Single-component calibration method just calibrates the six-component force sensor by loading one force at a time. When loading F_x,$C_{1j}(j = 1,2 \cdots 6)$can be got. The same goes for F_y to M_z.

$$F_x \rightarrow C_{11}, C_{12}, C_{13}, C_{14}, C_{15}, C_{16}$$
$$F_y \rightarrow C_{21}, C_{22}, C_{23}, C_{24}, C_{25}, C_{26}$$
$$F_z \rightarrow C_{31}, C_{32}, C_{33}, C_{34}, C_{35}, C_{36}$$
$$M_x \rightarrow C_{41}, C_{42}, C_{43}, C_{44}, C_{45}, C_{46}$$
$$M_y \rightarrow C_{51}, C_{52}, C_{53}, C_{54}, C_{55}, C_{56}$$
$$M_z \rightarrow C_{61}, C_{62}, C_{63}, C_{64}, C_{65}, C_{66}$$

In this way, the calibration matrix can be solved. In accordance with equation 3,

$$U_1 = C_{11} \cdot F_x + C_{21} \cdot F_y + C_{31} \cdot F_z + C_{41} \cdot M_x + C_{51} \cdot M_y + C_{61} \cdot M_z \quad (6)$$

The same goes for F_y to M_z. From equation 6, it can be known that U_i is a comprehensive embodiment of six loads loading one by one in single-component calibration.

2) Multi-component Calibration Method

Multi-component calibration method calibrates the six-component force sensor by loading more than one forces at the one time. Taking six-component calibration as an example, every time we can get a column matrix $F$with 6 elements and a column matrix$U$with 6 elements. For there are 36 elements in matrix C, 6 times six-component loading are needed. What's more, these 6 times six-component loading should not be in linear relationship.

Six-component calibration method just get C by getting six different equation 3, so U_i is a comprehensive embodiment of six loads loading at a time.

3. Theoretical Analysis

3.1 Difference in Different Calibration Method for Strain Gauge

In accordance with equation 1 and 2, we know that$\frac{\Delta L}{L}$is the root cause of$U_o$variation, so$\frac{\Delta L}{L}$in two different calibration methods are compared.

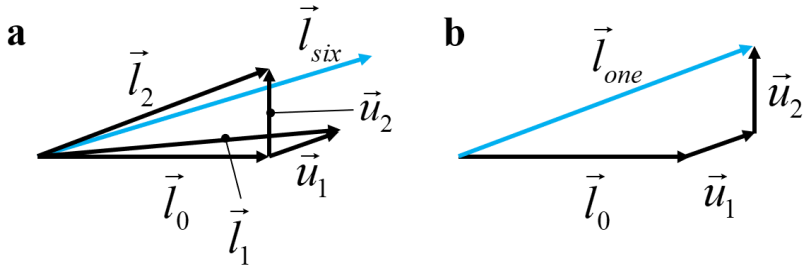

Figure 8. Deformation diagrammatic under calibration loads for one stick of the strain gauge grid. (a) Single-component Calibration (b) Multi-component Calibration

Taking one stick of the strain gauge grid as an example. As is shown in Figure 8.

$$\vec{l}_1 = \vec{l}_0 + \vec{u}_1 \quad (7)$$
$$\vec{l}_2 = \vec{l}_0 + \vec{u}_2 \quad (8)$$
$$\vec{l}_{single} = \vec{l}_1 + \vec{l}_2 \quad (9)$$
$$\vec{l}_{multi} = \vec{l}_0 + \vec{u}_1 + \vec{u}_2 \quad (10)$$
$$\frac{\Delta L}{L} = \frac{|\vec{l}| - |\vec{l}_0|}{|\vec{l}_0|} \quad (11)$$

Where $\vec{l}_0$ is a vector that its length l_0 is the same as the original length of one stick and its direction

ISSN 2616-5767 Vol.4, Issue 3: 33-51, DOI: 10.25236/AJETS.2021.040305

is along the stick prior to deformation. $\vec{u}_1$ is the displacement vector caused by one force or moment, whose length is $u_1.\vec{u}_2$ is the displacement vector caused by another force or moment, whose length is $u_2.\vec{l}_{single}$ is a vector that its length is the same as the length l_{single} of one stick inferior to deformation and its direction is along the stick inferior to deformation in single-component calibration method.$\vec{l}_{multi}$ is similar with $\vec{l}_{single}$ but it is in multi-component calibration method.

Equation 7 to 9 are inferred by single-component calibration. Equation 10 is inferred by multi-component calibration. From equation 7 to 10 we know that for single-component calibration,

$$|\vec{l}| - |\vec{l}_0| = l_1 - l_0 + l_2 - l_0 = \Delta l_1 + \Delta l_2 = \Delta L_{single}. \tag{12}$$

And for multi-component calibration

$$|\vec{l}| - |\vec{l}_0| = l_{multi} - l_0 = \Delta L_{multi}. \tag{13}$$

When $\Delta L_{single} = \Delta L_{multi}$, the results of single and multi-component calibration are the same, otherwise they are not the same.

In accordance with equation 7 to 10,

$$l_1{}^2 = l_0{}^2 + u_1{}^2 + 2l_0u_1\cos\theta_1 \tag{14}$$

$$l_2{}^2 = l_0{}^2 + u_2{}^2 + 2l_0u_2\cos\theta_2 \tag{15}$$

$$l_{multi}{}^2 = l_0{}^2 + u_1{}^2 + u_2{}^2 + 2l_0u_1\cos\theta_1 + 2l_0u_2\cos\theta_2 + 2u_1u_2\cos\theta_3 \tag{16}$$

Where θ_1 is the angle between $\vec{l}_0$ and $\vec{u}_1.\theta_2$ is the angle between $\vec{l}_0$ and $\vec{u}_2.\theta_3$ is the angle between $\vec{u}_1$ and $\vec{u}_2$. In accordance with equation 12 to 16,

$$\mathrm{l_{multi}}^2 - \mathrm{l_0}^2 = \mathrm{l_1}^2 - \mathrm{l_0}^2 + \mathrm{l_2}^2 - \mathrm{l_0}^2 + 2\mathrm{u_1u_2}\cos\theta_3 \tag{17}$$

$$(l_{multi} - l_0)(l_{multi} + l_0) = (l_1 - l_0)(l_1 + l_0) + (l_2 - l_0)(l_2 + l_0) + 2u_1u_2\cos\theta_3 \tag{18}$$

$$\Delta l_{multi}(\Delta l_{multi} + 2l_0) = \Delta l_1(\Delta l_1 + 2l_0) + \Delta l_2(\Delta l_2 + 2l_0) + 2u_1u_2\cos\theta_3 \tag{19}$$

$$\Delta l_{multi}{}^2 + 2l_0\Delta l_{multi} = \Delta l_1{}^2 + 2l_0\Delta l_1 + \Delta l_2{}^2 + 2l_0\Delta l_2 + 2u_1u_2\cos\theta_3 \tag{20}$$

In accordance with equation 20, only second-order elements $\Delta l_{multi}{}^2$,$\Delta l_1{}^2$,$\Delta l_2{}^2$and $2u_1u_2\cos\theta_3$ are ignored, can equation 21 to 22 be inferred.

$$2l_0\Delta l_{multi} = 2l_0\Delta l_1 + 2l_0\Delta l_2 \tag{21}$$

$$\Delta l_{multi} = \Delta l_1 + \Delta l_2 = \Delta l_{single} \tag{22}$$

Above is the example of two different direction loads loading on the sensor in two calibration methods. If there are six different direction loads F_x to M_z, equation 20 will be written as follows

$$\begin{aligned}\Delta l_{multi}{}^2 + 2l_0\Delta l_{multi} = {} & \Delta l_1{}^2 + 2l_0\Delta l_1 + \Delta l_2{}^2 + 2l_0\Delta l_2 + \Delta l_3{}^2 + 2l_0\Delta l_3 + \Delta l_4{}^2 + 2l_0\Delta l_4 + \Delta l_5{}^2 + \\ & 2l_0\Delta l_5 + \Delta l_6{}^2 + 2l_0\Delta l_6 + \sum_{i=2}^{6} 2u_1u_i\cos\theta_{i+5} + \sum_{j=3}^{6} 2u_2u_j\cos\theta_{j+9} + \\ & \sum_{k=4}^{6} 2u_3u_k\cos\theta_{k+13} + \sum_{m=5}^{6} 2u_4u_m\cos\theta_{m+15} + 2u_5u_6\cos\theta_{21}\end{aligned} \tag{23}$$

Only second-order elements $\Delta l_{multi}{}^2$,$\Delta l_1{}^2$ to $\Delta l_6{}^2$ and all elements after $2l_0\Delta l_6$ in equation 23 are ignored, can equation 24 be inferred.

$$\Delta l_{multi} = \Delta l_1 + \Delta l_2 + \Delta l_3 + \Delta l_4 + \Delta l_5 + \Delta l_6 = \Delta l_{single} \tag{24}$$

We can get the conclusion that results of single and multi-component calibration are not identical. Their difference is mainly caused by several second-order elements.

3.2 Difference in Different Calibration Method for Output Voltage

Strain gauges are inserted in the measuring bridge circuit. For resistance strain tire six-component force sensor with four column structure, the positions that strain gauges pasting on the elastic component and the method strain gauges inserted in measuring bridge for every measuring channel are almost the same. [27-28]

Figure 9 shows the diagrammatic of resistance strain tire six-component force sensor to be simulated.

ISSN 2616-5767 Vol.4, Issue 3: 33-51, DOI: 10.25236/AJETS.2021.040305

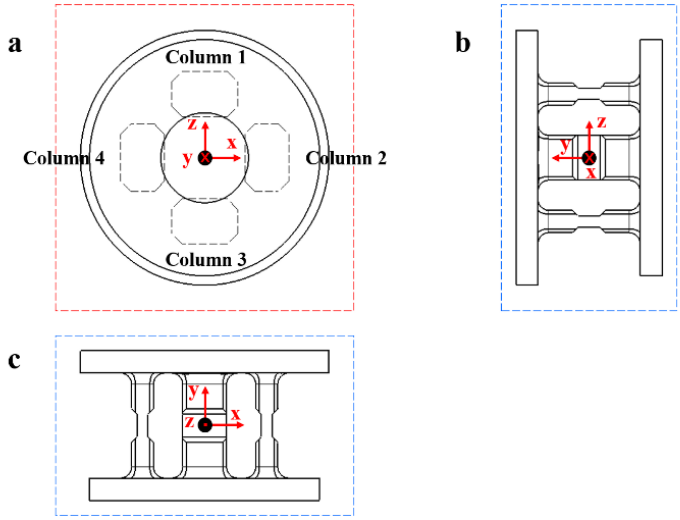

Figure 9. Three views of resistance strain tire six-component force sensor with four column structure. (a) Front view (b) Left view (3) Top view

Taking left view in Figure 9 to show the strain gauges positions of M_x measuring channel. They are all liner strain gauges and are inserted in the measuring bridge as Figure 7 shows.

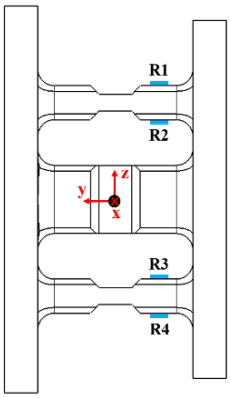

Figure 10. Strain gauges positions of M_x measuring channel

When M_y and F_x are loaded on sensor, there is a larger error between single and multi-component calibration results compared that for one strain gauge. Because when M_y is loaded,R_1 and R_2 on column 1 undergo deformations toward right, but R_3 and R_4 on column 2 undergo deformations toward left. When F_x is loaded,R_1, R_2 ,R_3 and R_4 all undergo deformations toward right.

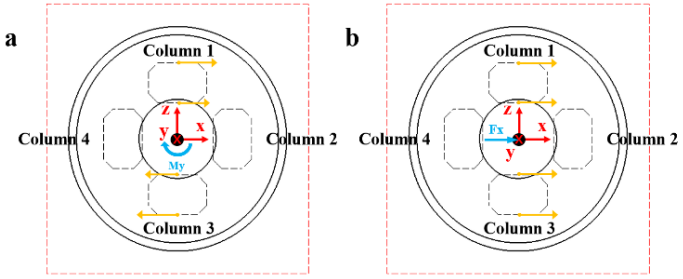

Figure 11. Elastic component deformations under load. (a) Loading M_y. (b) Loading F_x.

The elastic component deformation directions are as orange arrows shown in Figure 11. The strain gauges deformations are shown in Figure 12.

ISSN 2616-5767 Vol.4, Issue 3: 33-51, DOI: 10.25236/AJETS.2021.040305

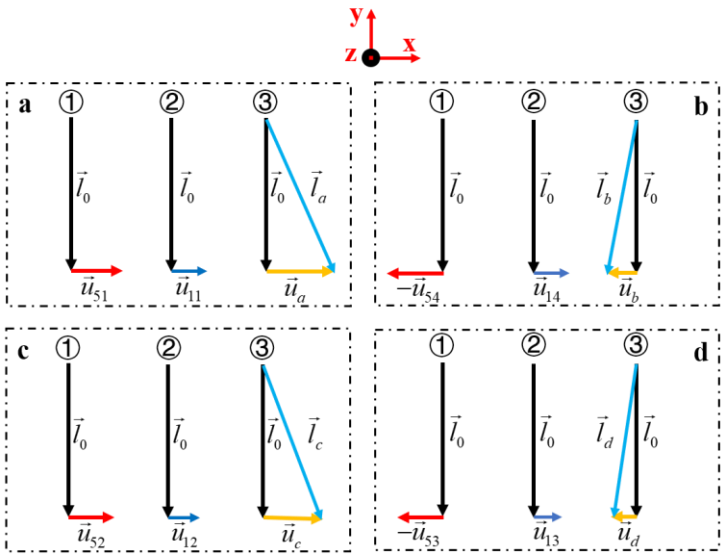

Figure 12. Strain gauge deformations under load. (a) Deformations of R_1. ① is the deformation under M_y. ② is the deformation under F_x. ③ is the deformation when M_y and F_x were loaded together. (b) Deformations of R_4. ① is the deformation under M_y. ② is the deformation under F_x. ③ is the deformation when M_y and F_x were loaded together. (c) Deformations of R_2. ① is the deformation under M_y. ② is the deformation under F_x. ③ is the deformation when M_y and F_x were loaded together. (d) Deformations of R_3. ① is the deformation under M_y. ② is the deformation under F_x. ③ is the deformation when M_y and F_x were loaded together.

From Figure 11 and 12 we know that in multi-component calibration method, deformation directions of R_1 and R_4 are different, though they are in symmetrical positions. Deformation directions of R_2 and R_3 are not the same either. To explain, assume that deformations caused by M_y and F_x are in the same line. Deformation equation of R_1 is

$$\vec{l}_a = \vec{l}_0 + \vec{u}_{51} + \vec{u}_{11}. \tag{25}$$

Deformation equation of R_4 is

$$\vec{l}_b = \vec{l}_0 - \vec{u}_{54} + \vec{u}_{14}. \tag{26}$$

Deformation equation of R_2 is

$$\vec{l}_c = \vec{l}_0 + \vec{u}_{52} + \vec{u}_{12}. \tag{27}$$

Deformation equation of R_3 is

$$\vec{l}_d = \vec{l}_0 - \vec{u}_{53} + \vec{u}_{13}. \tag{28}$$

According to the symmetry of sensor's structure,

$$|\vec{u}_{51}| = |-\vec{u}_{54}| = u_{51} = u_{54} \tag{29}$$

$$|\vec{u}_{11}| = |\vec{u}_{14}| = u_{11} = u_{14} \tag{30}$$

$$|\vec{u}_{52}| = |-\vec{u}_{53}| = u_{52} = u_{53} \tag{31}$$

$$|\vec{u}_{12}| = |\vec{u}_{13}| = u_{12} = u_{13} \tag{32}$$

When R_1 to R_4 were inserted in circuit,

$$U_o = \frac{KU_i}{4}\left(\frac{l_a - l_0}{l_0} + \frac{l_c - l_0}{l_0} - \frac{l_d - l_0}{l_0} - \frac{l_b - l_0}{l_0}\right) \neq 0. \tag{33}$$

It means that the crosstalk [29] of M_y and F_x working together to M_x channel is not zero in multi-component calibration.

But in single-component calibration, we get matrix C in accordance with the loads and output voltages. Whether M_y or F_x is loaded, strain gauges grids in R_1 to R_4 are all pulled, thought their deformations are the same as Figure 12 shows. Their output voltages are all positive. From this superficial phenomenon, deformations of R_1 and R_4 are considered in same direction. In fact, they were just both

ISSN 2616-5767 Vol.4, Issue 3: 33-51, DOI: 10.25236/AJETS.2021.040305

be pulled but not deform to the same direction. So, in single-component calibration method, deformation equations of R_1, R_2, R_3 and R_4 are considered as equation 34 to 38. Deformation equation of R_1 is

$$\vec{l}_a = \vec{l}_0 + \vec{u}_{51} + \vec{u}_{11}. \tag{34}$$

Deformation equation of R_4 is

$$\vec{l}_b = \vec{l}_0 + \vec{u}_{54} + \vec{u}_{14}. \tag{35}$$

Deformation equation of R_2 is

$$\vec{l}_c = \vec{l}_0 + \vec{u}_{52} + \vec{u}_{12}. \tag{36}$$

Deformation equation of R_3 is

$$\vec{l}_d = \vec{l}_0 + \vec{u}_{53} + \vec{u}_{13}. \tag{37}$$

Equation 29 to 32 still hold true in single-component calibration. When R_1 to R_4 were inserted in circuit,

$$U_o = \frac{KU_i}{4}\left(\frac{l_a - l_0}{l_0} + \frac{l_c - l_0}{l_0} - \frac{l_d - l_0}{l_0} - \frac{l_b - l_0}{l_0}\right) = 0. \tag{38}$$

It means that the crosstalk of M_y and F_x working together to M_x channel is zero in single-component calibration.

On the basis of analysis in this part, the conclusion that in single-component calibration method the crosstalk of M_y and F_x working together to M_x channel is zero but in multi-component calibration method it is not can be drew.

4. Simulation Experiments

Resistance strain tire six-component force sensor with four column structure was taken into simulation in this part.

Firstly, the sensor was meshed by using Hypermesh. In order to obtain higher simulation precision, mesh quality is important. Meshes in strain gauges pasting region were divided into regular hexahedral elements, whose sizes are 1*mm**1*mm**1*mm*. The transition region was divided into hexahedral elements or tetrahedron elements. (See Figure 13.)

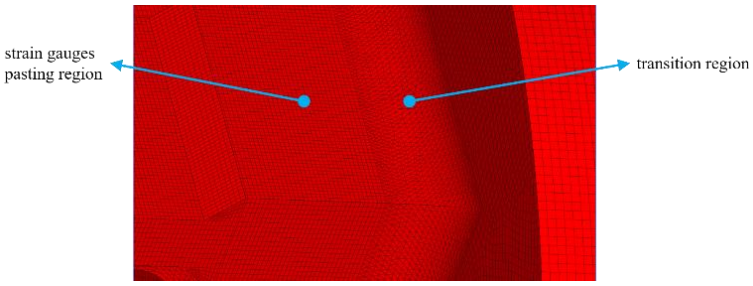

Figure 13. Meshes in strain gauges pasting region and transition region.

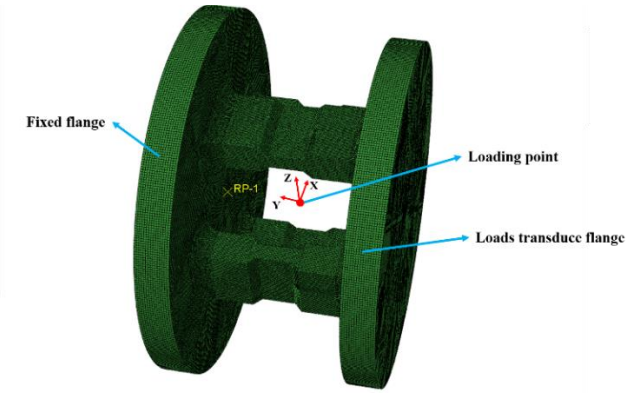

Figure 14. Boundary conditions.

ISSN 2616-5767 Vol.4, Issue 3: 33-51, DOI: 10.25236/AJETS.2021.040305

The simulation was realized by using Abaqus. Two flanges were set as rigid bodies to realize ideal deformation. [30] Flange on one side was fixed in six degrees and loads were transduced by flange on the other side. For the convenience of loading, a reference point was created at the origin of coordinate. (See Figure 14.)

4.1 Difference in Different Calibration Method for Strain Gauge

In accordance with equation 33 and 38,l_a to l_d should be solved to compare the difference in these two methods. In single-component calibration,l_a to l_d were expressed as $l_{asingle}$ to $l_{dsingle}$. In multi-component calibration, l_a to l_d were expressed as l_{amulti} to l_{dmulti}. What's different between l_a to l_d and $l_{asingle}$ to $l_{dsingle}$,l_{amulti} to l_{dmulti} is that one strain gauge has many sticks, here taking four of them to get the result, not just one. Figure 15 is the diagrammatic.

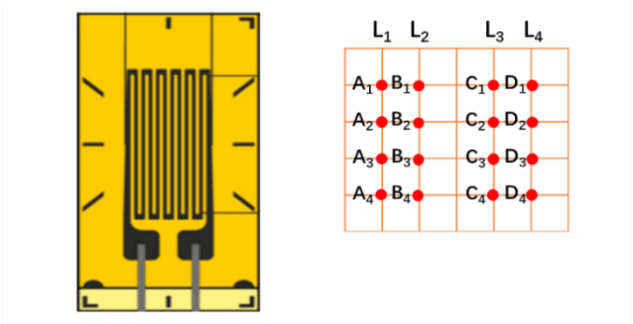

Figure 15. Strain gauge and analyzing nodes.

Taking four nodes on each stick into simulation, the size of every mesh is 1mm*1mm*1mm. The original length of the strain gauge is 12mm. The length inferior to deformation was calculated by the three-dimensional coordinates of nodes A_1 to A_4, B_1 to B_4 , C_1 to C_4 and D_1 to D_4.

Single-component Calibration

Six times of simulations were carried out. Every time put one load on loading point. $F_x = 32000N$, $F_y = 24000N$, $F_z = 32000N$, $M_x = 12000000N \cdot mm$, $M_y = 12000000N \cdot mm$ and $M_z = 12000000N \cdot mm$. The simulation strain nephograms are shown in Figure 16.

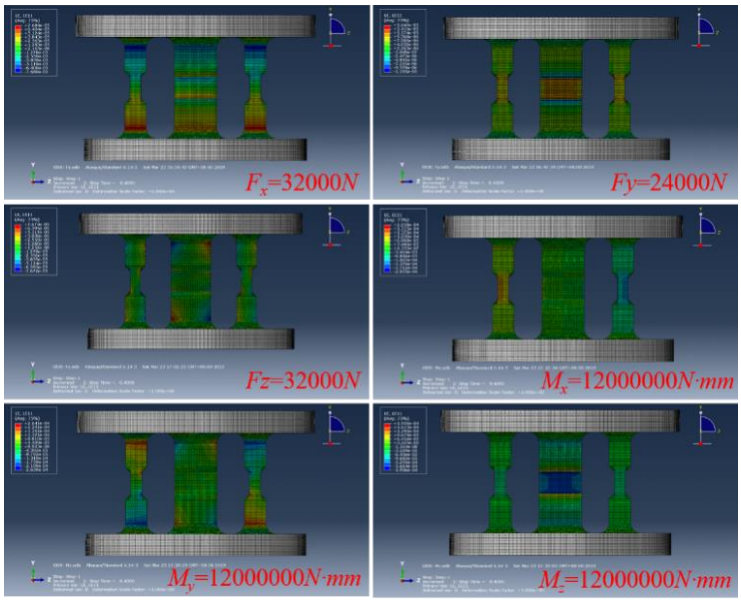

Figure 16. Simulation strain nephograms. Loads are as shown in every picture.

Deformations of R_1, R_2, R_3 and R_4 in single-component calibration are shown in table 1 to 4.

ISSN 2616-5767 Vol.4, Issue 3: 33-51, DOI: 10.25236/AJETS.2021.040305

Table 1. Strain gauge deformation of R_1 in single-component calibration method.

Load	l_0	$l_{asingle}$	$l_{asingle} - l_0$
$F_x = 32000N$	12mm	11.99999926mm	-0.00000074mm
$F_y = 24000N$	12mm	11.99981200mm	-0.00018800mm
$F_z = 32000N$	12mm	12.00124621mm	0.00124621mm
$M_x = 12000000N \cdot mm$	12mm	12.00226875mm	0.00226875mm
$M_y = 12000000N \cdot mm$	12mm	12.00000566mm	0.00000566mm
$M_z = 12000000N \cdot mm$	12mm	11.99999971mm	-0.00000029mm

From table 1, the sum of $l_{asingle} - l_0$ for R_1 under six single-component loads is

$$\Delta L_{R_1 single} = 0.00333159mm. \tag{39}$$

Table 2. Strain gauges deformations of R_2 in single-component calibration method.

Load	l_0	$l_{csingle}$	$l_{csingle} - l_0$
$F_x = 32000N$	12mm	12.00000026mm	0.00000026mm
$F_y = 24000N$	12mm	11.99981200mm	-0.00018800mm
$F_z = 32000N$	12mm	11.99875221mm	-0.00124779mm
$M_x = 12000000N \cdot mm$	12mm	12.00191484mm	0.00191484mm
$M_y = 12000000N \cdot mm$	12mm	11.999997602mm	-0.00000240mm
$M_z = 12000000N \cdot mm$	12mm	11.999999710mm	-0.00000029mm

From table 2, the sum of $l_{csingle} - l_0$ forR_2under six single-component loads is

$$\Delta L_{R_2 single} = 0.00047663mm. \tag{40}$$

Table 3. Strain gauges deformations of R_3 in single-component calibration method.

Load	l_0	$l_{dsingle}$	$l_{dsingle} - l_0$
$F_x = 32000N$	12mm	12.00000026mm	0.00000026mm
$F_y = 24000N$	12mm	11.99981200mm	-0.00018800mm
$F_z = 32000N$	12mm	12.00124821mm	0.00124821mm
$M_x = 12000000N \cdot mm$	12mm	11.99808084mm	-0.00191916mm
$M_y = 12000000N \cdot mm$	12mm	11.99999760mm	-0.00000240mm
$M_z = 12000000N \cdot mm$	12mm	11.99999971mm	-0.00000029mm

From table 3, the sum of $l_{dsingle} - l_0$ for R_3 under six single-component loads is

$$\Delta L_{R_3 single} = -0.00086137mm. \tag{41}$$

Table 4. Strain gauges deformations of R_4 in single-component calibration method.

Load	l_0	$l_{bsingle}$	$l_{bsingle} - l_0$
$F_x = 32000N$	12mm	11.99999926mm	-0.00000074mm
$F_y = 24000N$	12mm	11.99981200mm	-0.00018800mm
$F_z = 32000N$	12mm	11.99875221mm	-0.00124779mm
$M_x = 12000000N \cdot mm$	12mm	11.99773876mm	-0.00226124mm
$M_y = 12000000N \cdot mm$	12mm	12.00000566mm	0.00000566mm
$M_z = 12000000N \cdot mm$	12mm	11.99999971mm	-0.00000029mm

From table 4, the sum of $l_{bsingle} - l_0$ for R_4 under six single-components loads is

$$\Delta L_{R_4 single} = -0.00369240mm. \tag{42}$$

Multi-component Calibration

One time of simulation was carried out. Put six loads on loading point at one time. $F_x = 32000N$, $F_y = 24000N$, $F_z = 32000N$, $M_x = 12000000N \cdot mm$, $M_y = 12000000N \cdot mm$ and $M_z = 12000000N \cdot mm$.The simulation strain nephogram is shown in Figure 17.

ISSN 2616-5767 Vol.4, Issue 3: 33-51, DOI: 10.25236/AJETS.2021.040305

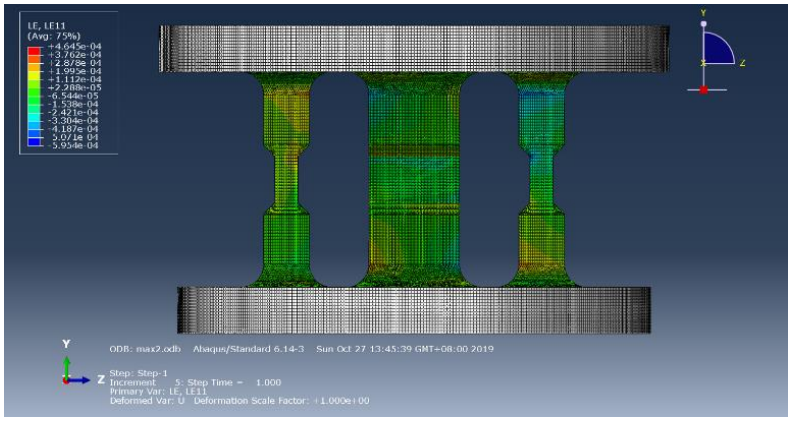

Figure 17. Simulation strain nephogram. Six loads are loaded at the one time.

Deformations of R_1, R_2, R_3 and R_4 in multi-component calibration are shown in table 5 to 8.

Table 5. Strain gauge deformation of R_1 in multi-component calibration method.

Load	l_0	l_{amulti}	$l_{amulti} - l_0$
$F_x = 32000N$ $F_y = 24000N$ $F_z = 32000N$ $M_x = 12000000N \cdot mm$ $M_y = 12000000N \cdot mm$ $M_z = 12000000N \cdot mm$	12mm	12.00333003mm	0.00333003mm

From table 5, $l_{amulti} - l_0$ for R_1 under multi-component loads is

$$\Delta L_{R_1 multi} = 0.00333003mm. \tag{43}$$

Table 6. Strain gauge deformation of R_2 in multi-component calibration method.

Load	l_0	l_{cmulti}	$l_{cmulti} - l_0$
$F_x = 32000N$ $F_y = 24000N$ $F_z = 32000N$ $M_x = 12000000N \cdot mm$ $M_y = 12000000N \cdot mm$ $M_z = 12000000N \cdot mm$	12mm	12.00048203mm	0.00048203mm

From table 6, $l_{cmulti} - l_0$ for R_2 under multi-component loads is

$$\Delta L_{R_2 multi} = 0.00048203mm. \tag{44}$$

Table 7. Strain gauge deformation of R_3 in multi-component calibration method.

Load	l_0	l_{dmulti}	$l_{dmulti} - l_0$
$F_x = 32000N$ $F_y = 24000N$ $F_z = 32000N$ $M_x = 12000000N \cdot mm$ $M_y = 12000000N \cdot mm$ $M_z = 12000000N \cdot mm$	12mm	11.99913822mm	-0.00086178mm

From table 7, $l_{dmulti} - l_0$ for R_3 under multi-component loads is

$$\Delta L_{R_3 multi} = -0.00086178mm. \tag{45}$$

Table 8. Strain gauge deformation of R_4 in multi-component calibration method.

Load	l_0	l_{bmulti}	$l_{bmulti} - l_0$
$F_x = 32000N$ $F_y = 24000N$ $F_z = 32000N$ $M_x = 12000000N \cdot mm$ $M_y = 12000000N \cdot mm$ $M_z = 12000000N \cdot mm$	12mm	11.99631224mm	-0.00368776mm

From table 8, $l_{bmulti} - l_0$ for R_4 under multi-component loads is

$$\Delta L_{R_4 multi} = -0.00368776mm. \tag{46}$$

So, the relative error between single and multi-component calibration for one strain gauge (taking result of multi-component calibration result as the benchmark) is

$$E_{strain1} = \frac{|\Delta L_{R_1 multi} - \Delta L_{R_1 single}|}{\Delta L_{R_1 multi}} \times 100\% = 0.05\%, \tag{47}$$

$$E_{strain2} = \frac{|\Delta L_{R_2 multi} - \Delta L_{R_2 single}|}{\Delta L_{R_2 multi}} \times 100\% = 1.12\%, \tag{48}$$

$$E_{strain3} = \frac{|\Delta L_{R_3 multi} - \Delta L_{R_3 single}|}{\Delta L_{R_3 multi}} \times 100\% = 0.05\%, \tag{49}$$

ISSN 2616-5767 Vol.4, Issue 3: 33-51, DOI: 10.25236/AJETS.2021.040305

$$E_{strain4} = \frac{|\Delta L_{R_4 multi} - \Delta L_{R_4 single}|}{\Delta L_{R_4 multi}} \times 100\% = 1.15\%. \quad (50)$$

In accordance with the simulation results of this part, the conclusion that results of single and multi-component calibration are not identical is confirmed.

4.2 Difference in Different Calibration Method for Output Voltage

Equation 33 and 38 are different in the part in brackets. So, equation 51 and 52 are used here to compare the difference between M_y and F_x working in single or multi-component calibration method.

$$\Delta L_{single} = \Delta L_{R_1 single} + \Delta L_{R_2 single} - \Delta L_{R_3 single} - \Delta L_{R_4 single} \quad (51)$$

$$\Delta L_{multi} = \Delta L_{R_1 multi} + \Delta L_{R_2 multi} - \Delta L_{R_3 multi} - \Delta L_{R_4 multi} \quad (52)$$

Single-component Calibration

Twelve times of simulations were carried out. Every time one load was put on loading point. $F_x = 16000N, 32000N, 48000N, 64000N$ and $80000N$, $M_y = 6000000N \cdot mm, 12000000N \cdot mm, 18000000N \cdot mm, 24000000N \cdot mm$ and $30000000N \cdot mm$. The simulation strain nephograms are shown in Figure 18 and 19.

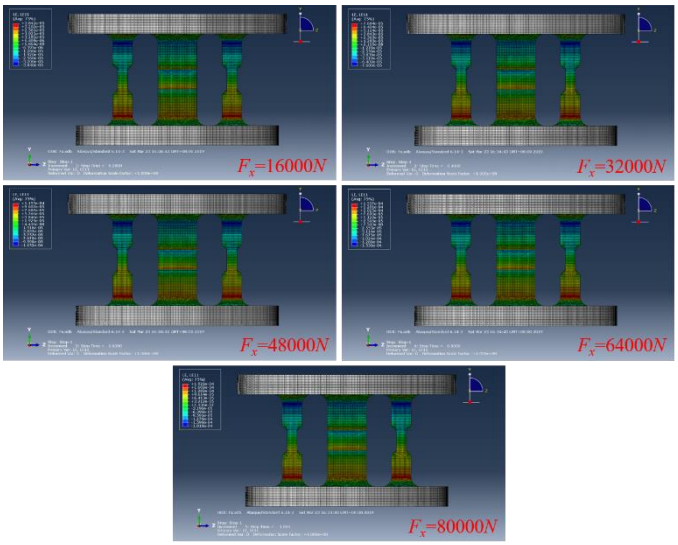

Figure 18. Simulation strain nephogram under F_x. Loads are as shown in every picture.

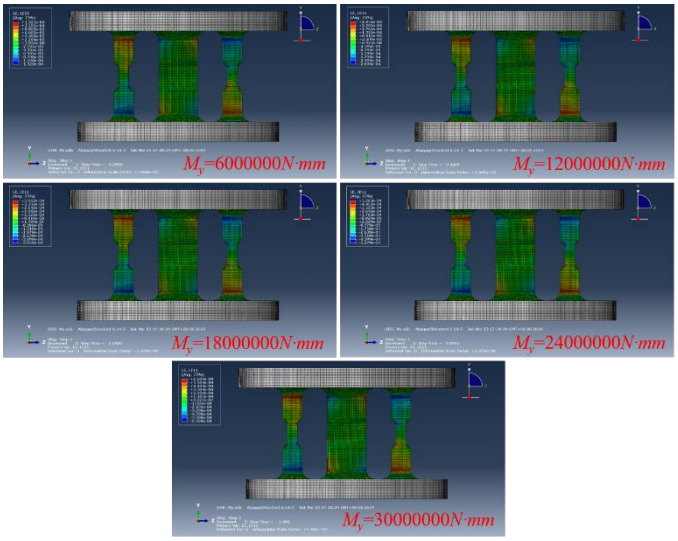

Figure 19. Simulation strain nephogram under M_y. Loads are as shown in every picture.

Deformations of R_1, R_2, R_3 and R_4 in single-component calibration are shown in table 9 to 16.

ISSN 2616-5767 Vol.4, Issue 3: 33-51, DOI: 10.25236/AJETS.2021.040305

Table 9. Strain gauge deformation of R_1 in single-component calibration method.

Load	l_0	$l_{asingle}$	$l_{asingle} - l_0$
$F_x = 16000N$	12mm	12.00000007mm	0.00000007mm
$F_x = 32000N$	12mm	11.99999926mm	-0.00000074mm
$F_x = 48000N$	12mm	12.00000058mm	0.00000058mm
$F_x = 64000N$	12mm	12.00000003mm	0.00000003mm
$F_x = 80000N$	12mm	12.00000062mm	0.00000062mm
$M_y = 6000000N \cdot mm$	12mm	12.00000267mm	0.00000267mm
$M_y = 12000000N \cdot mm$	12mm	12.00000566mm	0.00000566mm
$M_y = 18000000N \cdot mm$	12mm	12.00001498mm	0.00001498mm
$M_y = 24000000N \cdot mm$	12mm	12.00002463mm	0.00002463mm
$M_y = 30000000N \cdot mm$	12mm	12.00003761mm	0.00003761mm

From table 9, the sum of $l_{asingle} - l_0$ for R_1 under F_x and M_y single-component loads are shown in table 10.

Table 10. Strain gauge deformation of R_1 in single-component calibration method. The results F_x and M_y causing are added together.

Load	$\Delta L_{R_1 single}$
$F_x = 16000N$ $M_y = 6000000N \cdot mm$	0.00000273mm
$F_x = 32000N$ $M_y = 12000000N \cdot mm$	0.00000492mm
$F_x = 48000N$ $M_y = 18000000N \cdot mm$	0.00001556mm
$F_x = 64000N$ $M_y = 24000000N \cdot mm$	0.00002466mm
$F_x = 80000N$ $M_y = 30000000N \cdot mm$	0.00003823mm

Table 11. Strain gauge deformation of R_2 in single-component calibration method.

Load	l_0	$l_{csingle}$	$l_{csingle} - l_0$
$F_x = 16000N$	12mm	12.00000006mm	0.00000006mm
$F_x = 32000N$	12mm	12.00000026mm	0.00000026mm
$F_x = 48000N$	12mm	12.00000058mm	0.00000058mm
$F_x = 64000N$	12mm	12.00000003mm	0.00000003mm
$F_x = 80000N$	12mm	12.00000061mm	0.00000061mm
$M_y = 6000000N \cdot mm$	12mm	11.99999940mm	-0.00000060mm
$M_y = 12000000N \cdot mm$	12mm	11.99999760mm	-0.00000240mm
$M_y = 18000000N \cdot mm$	12mm	11.99999460mm	-0.00000540mm
$M_y = 24000000N \cdot mm$	12mm	11.99999241mm	-0.00000759mm
$M_y = 30000000N \cdot mm$	12mm	11.99998901mm	-0.00001099mm

From table 11, the sum of $l_{csingle} - l_0$ for R_2 under F_x and M_y single-component loads are shown in table 12.

Table 12. Strain gauge deformation of R_2 in single-component calibration method. The results F_x and M_y causing are added together.

Load	$\Delta L_{R_2 single}$
$F_x = 16000N$ $M_y = 6000000N \cdot mm$	-0.00000054mm
$F_x = 32000N$ $M_y = 12000000N \cdot mm$	-0.00000214mm
$F_x = 48000N$ $M_y = 18000000N \cdot mm$	-0.00000482mm
$F_x = 64000N$ $M_y = 24000000N \cdot mm$	-0.00000756mm
$F_x = 80000N$ $M_y = 30000000N \cdot mm$	-0.00001038mm

ISSN 2616-5767 Vol.4, Issue 3: 33-51, DOI: 10.25236/AJETS.2021.040305

Table 13. Strain gauge deformation of R_3 in single-component calibration method.

Load	l_0	$l_{dsingle}$	$l_{dsingle} - l_0$
$F_x = 16000N$	12mm	12.00000006mm	0.00000006mm
$F_x = 32000N$	12mm	12.00000026mm	0.00000026mm
$F_x = 48000N$	12mm	12.00000058mm	0.00000058mm
$F_x = 64000N$	12mm	12.00000003mm	0.00000003mm
$F_x = 80000N$	12mm	12.00000061mm	0.00000061mm
$M_y = 6000000N \cdot mm$	12mm	11.99999940mm	-0.00000060mm
$M_y = 12000000N \cdot mm$	12mm	11.99999760mm	-0.00000240mm
$M_y = 18000000N \cdot mm$	12mm	11.99999460mm	-0.00000540mm
$M_y = 24000000N \cdot mm$	12mm	11.99999241mm	-0.00000759mm
$M_y = 30000000N \cdot mm$	12mm	11.99998901mm	-0.00001099mm

From table 13, the sum of $l_{dsingle} - l_0$ for R_3 under F_x and M_y single-component loads are shown in table 14.

Table 14. Strain gauge deformation of R_3 in single-component calibration method. The results F_x and M_y causing are added together.

Load	$\Delta L_{R_2 single}$
$F_x = 16000N\ M_y = 6000000N \cdot mm$	-0.00000054mm
$F_x = 32000N\ M_y = 12000000N \cdot mm$	-0.00000214mm
$F_x = 48000N\ M_y = 18000000N \cdot mm$	-0.00000482mm
$F_x = 64000N\ M_y = 24000000N \cdot mm$	-0.00000756mm
$F_x = 80000N\ M_y = 30000000N \cdot mm$	-0.00001038mm

Table 15. Strain gauge deformation of R_4 in single-component calibration method.

Load	l_0	$l_{bsingle}$	$l_{bsingle} - l_0$
$F_x = 16000N$	12mm	12.00000007mm	0.00000007mm
$F_x = 32000N$	12mm	11.99999926mm	-0.00000074mm
$F_x = 48000N$	12mm	12.00000058mm	0.00000058mm
$F_x = 64000N$	12mm	12.00000003mm	0.00000003mm
$F_x = 80000N$	12mm	12.00000062mm	0.00000062mm
$M_y = 6000000N \cdot mm$	12mm	12.00000267mm	0.00000267mm
$M_y = 12000000N \cdot mm$	12mm	12.00000566mm	0.00000566mm
$M_y = 18000000N \cdot mm$	12mm	12.00001498mm	0.00001498mm
$M_y = 24000000N \cdot mm$	12mm	12.00002463mm	0.00002463mm
$M_y = 30000000N \cdot mm$	12mm	12.00003761mm	0.00003761mm

From table 15, the sum of $l_{bsingle} - l_0$ for R_4 under F_x and M_y single-component loads are shown in table 16.

Table 16. Strain gauge deformation of R_4 in single-component calibration method. The results F_x and M_y causing are added together.

Load	$\Delta L_{R_1 single}$
$F_x = 16000N\ M_y = 6000000N \cdot mm$	0.00000273mm
$F_x = 32000N\ M_y = 12000000N \cdot mm$	0.00000492mm
$F_x = 48000N\ M_y = 18000000N \cdot mm$	0.00001556mm
$F_x = 64000N\ M_y = 24000000N \cdot mm$	0.00002466mm
$F_x = 80000N\ M_y = 30000000N \cdot mm$	0.00003823mm

According to table 9 to 16,ΔL_{single} can be got.

ISSN 2616-5767 Vol.4, Issue 3: 33-51, DOI: 10.25236/AJETS.2021.040305

Table 17. ΔL_{single} got from single-component calibration method.

Load	ΔL_{single}
$F_x = 16000N$ $M_y = 6000000N \cdot mm$	0mm
$F_x = 32000N$ $M_y = 12000000N \cdot mm$	0mm
$F_x = 48000N$ $M_y = 18000000N \cdot mm$	0mm
$F_x = 64000N$ $M_y = 24000000N \cdot mm$	0mm
$F_x = 80000N$ $M_y = 30000000N \cdot mm$	0mm

We can get the conclusion that in single-component calibration method, crosstalk of F_x and M_y to M_x is zero.

Multi-component Calibration

Six times of simulations were carried out. Every time put two loads on loading point.

① $F_x = 16000N, M_y = 6000000N \cdot mm$

② $F_x = 32000N, M_y = 12000000N \cdot mm$

③ $F_x = 48000N, M_y = 18000000N \cdot mm$

④ $F_x = 64000N, M_y = 24000000N \cdot mm$

⑤$F_x = 80000N, M_y = 30000000N \cdot mm.$

The simulation strain nephograms are shown in Figure 20.

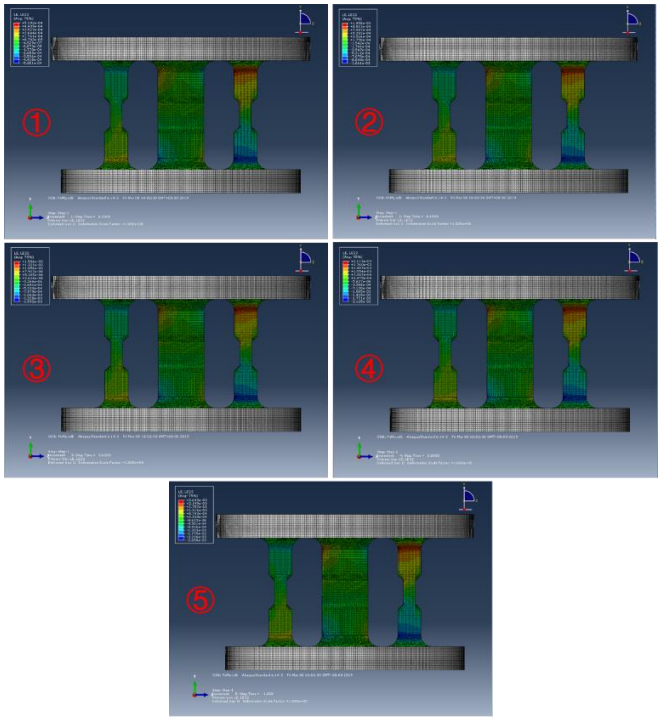

Figure 20. Simulation strain nephogram under five kinds of loads.

Deformations of R_1, R_2, R_3 and R_4 in multi-component calibration are shown in table 18 to 21.

Table 18. Strain gauge deformation of R_1 in multi-component calibration method.

Load	$\Delta L_{R_1 multi}$
$F_x = 16000N$ $M_y = 6000000N \cdot mm$	0.00000214mm
$F_x = 32000N$ $M_y = 12000000N \cdot mm$	0.00001057mm
$F_x = 48000N$ $M_y = 18000000N \cdot mm$	0.00002129mm
$F_x = 64000N$ $M_y = 24000000N \cdot mm$	0.00003829mm
$F_x = 80000N$ $M_y = 30000000N \cdot mm$	0.00006158mm

ISSN 2616-5767 Vol.4, Issue 3: 33-51, DOI: 10.25236/AJETS.2021.040305

Table 19. Strain gauge deformation of R_2 in multi-component calibration method.

Load	$\Delta L_{R_2 multi}$
$F_x = 16000N$ $M_y = 6000000N \cdot mm$	-0.00000121mm
$F_x = 32000N$ $M_y = 12000000N \cdot mm$	-0.00000285mm
$F_x = 48000N$ $M_y = 18000000N \cdot mm$	-0.00000692mm
$F_x = 64000N$ $M_y = 24000000N \cdot mm$	-0.00000942mm
$F_x = 80000N$ $M_y = 30000000N \cdot mm$	-0.00001534mm

Table 20. Strain gauge deformation of R_3 in multi-component calibration method.

Load	$\Delta L_{R_3 multi}$
$F_x = 16000N$ $M_y = 6000000N \cdot mm$	0.00000014mm
$F_x = 32000N$ $M_y = 12000000N \cdot mm$	-0.00000043mm
$F_x = 48000N$ $M_y = 18000000N \cdot mm$	-0.00000271mm
$F_x = 64000N$ $M_y = 24000000N \cdot mm$	-0.00000471mm
$F_x = 80000N$ $M_y = 30000000N \cdot mm$	-0.00000742mm

Table 21. Strain gauge deformation of R_4 in multi-component calibration method.

Load	$\Delta L_{R_4 multi}$
$F_x = 16000N$ $M_y = 6000000N \cdot mm$	0.00000032mm
$F_x = 32000N$ $M_y = 12000000N \cdot mm$	0.00000126mm
$F_x = 48000N$ $M_y = 18000000N \cdot mm$	0.00000683mm
$F_x = 64000N$ $M_y = 24000000N \cdot mm$	0.00001004mm
$F_x = 80000N$ $M_y = 30000000N \cdot mm$	0.00001587mm

According to table 18 to 21,ΔL_{multi} can be got.

Table 22. ΔL_{multi} got from multi-component calibration method.

Load	ΔL_{multi}
$F_x = 16000N$ $M_y = 6000000N \cdot mm$	0.00000047mm
$F_x = 32000N$ $M_y = 12000000N \cdot mm$	0.00000689mm
$F_x = 48000N$ $M_y = 18000000N \cdot mm$	0.00001024mm
$F_x = 64000N$ $M_y = 24000000N \cdot mm$	0.00002355mm
$F_x = 80000N$ $M_y = 30000000N \cdot mm$	0.00003779mm

We can get the conclusion that in multi-component calibration method, crosstalk of F_x and M_y to M_x is not zero.

In fact, the crosstalk of F_x and M_y to M_x in multi-component calibration method was proved to be 0.01% to 0.18%.

In accordance with the simulation results of this part, the conclusion that in single-component calibration method the crosstalk of M_y and F_x working together to M_x channel is zero but in multi-component calibration method it is not is confirmed.

5. A More Reasonable Method to Improve the Calibration Precision

The tire is the only component in contact with the road while automobiles are running. As is shown in Figure 21, tires usually transfer three forces and three moments at the same time, they are caused by many input factors. [31] For tire six-component force sensor, the best calibration way is to calibrate it under conditions it works.

ISSN 2616-5767 Vol.4, Issue 3: 33-51, DOI: 10.25236/AJETS.2021.040305

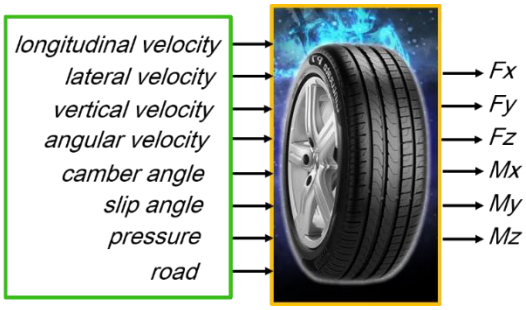

Figure 21. Tire's input factors and output forces.

In accordance with the results above, we know that difference between single and multi-component calibration for one strain gauge is inevitable, and that for voltage output is also unavoidable. Tire six-component force sensor usually has the precision between 0.25% to 3% [32-33], so, a crosstalk whose value is 0.18% in fact has a large influence. In order to get a tire six-component force sensor with higher precision working under multi forces, multi-component calibration is a better method than single-component method.

6. Conclusions

In this study, we compared the difference between single and multi-component calibration results of tire six-component force sensor. Different results mainly appear in measuring of strain gauge and certain output voltage channel. The study was carried out in theoretical analysis and simulation experiments. Simulation experiences confirmed the results referred by theoretical analysis. Considering the conditions under which the tire works, multi-component calibration is a better method than single-component method, for it can get results with higher precision.

In future work, we will focus on the elastic component structures and gauges positions. The difference offered in this study of two calibration methods might can be reduced. The multi-component calibration equipment will also be studied because it can be helpful to get a six-component force sensor with higher precision.

Acknowledgements

This work was supported by Liuzhou Science and Technology Project [NO. 2018AA20501].

References

[1] Guo Konghui, "Vehicle Tire Dynamics," (Beijing, Science Press, 2018), ISBN 978-7-03-059128-9
[2] Pacejka, H.B., "Tyre and Vehicle Dynamics, Third Edition," (Butterworth-Heinemann, 2012), ISBN: 978-0-08-097016-5
[3] Gipser, and M. "FTire – the tire simulation model for all applications related to vehicle dynamics." Vehicle System Dynamics 45. sup1 (2007): 139-151. doi: 10.1080/00423110801899960
[4] Wang Dong, "Research on Decoupling Theory and Technology of Automobile Wheel Force Measurement," Ph.D. thesis, School of Instrument Science and Engineering, Southeast University, Nanjing, 2016
[5] Feng, Lihang, et al. "Design and optimization of a self-decoupled six-axis wheel force transducer for a heavy truck." Proceedings of the Institution of Mechanical Engineers, Part D: Journal of Automobile Engineering 229.12 (2015): 1585-1610. doi: 10.1177/0954407014566439
[6] Sun, Yongjun, et al. "Design and optimization of a novel six-axis force/torque sensor for space robot." Measurement 65 (2015): 135-148. doi: 10.1016/j.measurement.2015.01.005
[7] Xu Zhengzheng, "Design and Implementation of Wheel Force Sensor with Inertial Decoupling Function, "master's thesis, School of Instrument Science and Engineering, Southeast University, Nanjing, 2017
[8] Li, Ying Jun, et al. "A novel parallel piezoelectric six-axis heavy force/torque sensor." Measurement 42.5(2009): 730-736. doi: 10.1016/j.measurement.2008.12.005
[9] Wang, Zhijun, et al. "Optimal design and experiment research of a fully pre-stressed six-axis force/torque sensor." Measurement 46.6(2013):2013-2021. doi: 10.1016/j.measurement.2013.03.003

ISSN 2616-5767 Vol.4, Issue 3: 33-51, DOI: 10.25236/AJETS.2021.040305

[10] Pytka, J., "A Wheel Dynamometer for Off-Road Vehicles Testing," SAE Technical Paper 2008-01-0783, 2008, doi: 10.4271/2008-01-0783.

[11] Yao, Jiantao, et al. "Task-oriented design method and research on force compliant experiment of six-axis wrist force sensor." Mechatronics 35(2016):109-121. doi: 10.1016/j.mechatronics.2016.01.007

[12] Chen, Danfeng, A. Song, and A. Li. "Design and Calibration of a Six-axis Force/torque Sensor with Large Measurement Range Used for the Space Manipulator." Procedia Engineering 99 (2015): 1164-1170. doi: 10.1016/j.proeng.2014.12.699

[13] Ballo F, et al. "Advances in Force and Moments Measurements by an Innovative Six-axis Load Cell." Experimental Mechanics 54.4(2014):571-592. doi: 10.1007/s11340-013-9824-4

[14] Pan Ying, "Research on Six-dimensional Force Sensor Calibration System Based on Stewart Platform", master's thesis, Apparatus Science and Engineering Department, Dalian Jiaotong University, Dalian, 2017

[15] Nitsche, J., et al. "Measurement uncertainty evaluation of a hexapod-structured calibration device for multi-component force and moment sensors." Metrologia 54.2(2017): 171-183.doi: 10.1088/1681-7575/aa5b66

[16] "Calibration services" https://www.kistler.com/?type=669&fid=319&model=download&callee=frontend

[17] Zhang Jingzhu, "Study on Design Principle of Special Six-component Force Sensors," Ph.D. thesis, College of Ordnance Science and Technology, Nanjing University of Science and Technology, Nanjing, 2008

[18] Guo Konghui, Jin Lingge, and Lu dang. "Application of UniTire in vehicle dynamics simulation." Journal of Jilin University (Engineering) v.39.S2: 241-245.

[19] Railway Engineering Research Institute of China Academy of Railway Sciences, "Resistance Strain Pressure Transducer," (China Railway Publishing House, Beijing) 1979.

[20] Li Yan, Li Xine and Pei Dongxing. "Strain pressure sensor and its application circuit design." Measurement and Testing Techniques 12(2007).

[21] Yin FuYan. "Research on Resistance Strain Gage and Strain Transfer Principle." Science and technology application 2(2010): 1-8.

[22] https://www.hbm.com/en/4707/series-m-strain-gauges-at-an-extended-strain-level/#accordion-297653-539

[23] Akbari, Hossein, and A. Kazerooni. "Improving the coupling errors of a Maltese cross-beams type six-axis force/moment sensor using numerical shape-optimization technique." Measurement 126.C (2018): 342-355. doi: 10.1016/j.measurement. 2018.05.074

[24] Qiaokang, Liang, et al. "Design and Analysis of a Sensor System for Cutting Force Measurement in Machining Processes." Sensors 16.1(2016):70-. doi: 10.3390/s16010070

[25] Palli, G., et al. "Development of an optoelectronic 6-axis force/torque sensor for robotic applications." Sensors and Actuators A: Physical 220(2014): 333-346. doi: 10.1016/j.sna.2014.09.023

[26] Hai-Bin, L. I., et al. "New Calibration Method of Six-Axis Force Sensor Based on Stewart Platform." Chinese Journal of Sensors and Actuators 19.1(2006):132-136. doi: 10.1016/S1005-8885(07)60041-7

[27] Huang Jichang, Xu Qiaoyu and Zhang Haigui. "Working Principle and Application Example of Sensor," (Posts & Telecom Press, Beijing) 1998.

[28] Huge W. Larsen, Carl E. Talaski, "Multi-axis Wheel Load Transducer," U.S. Patent 6,324,919, Dec. 4, 2001.

[29] Hong, Daewoong, C. Li, and J. Jeong. "A Crosstalk Compensation of a Multi-axis ForceTorque Sensor Based on the Least Squares Method Using LabVIEW." Fourth International Conference on Computational & Information Sciences IEEE, 2012. doi: 10.1109/ICCIS.2012.12

[30] Gao Fei, "Numerical calculation and analysis of a six-component force transducer," master's thesis, Transport College, Wuhan University of Technology, Wuhan, 2006

[31] Guo Konghui, "Vehicle Handling Dynamics," (Cahngchun, Jilin Science and Technology Press, 1991), ISBN 978-7-53-840859-1

[32] http://www.msc-cn.com/products/transducers/wheel-force-transducers/

[33] https://www.kistler.com/zh/applications/automotive-research-test/vehicle-dynamics-durability/tire-testing/